Journal of Power Sources 195 (2010) 6732–6739

Contents lists available at ScienceDirect

Journal of Power Sources

journal homepage: www.elsevier.com/locate/jpowsour

Optimum start-up strategies for direct internal reforming molten carbonate fuel cell systems

W. Wu [a,*], J.J. Luo [a], J.J. Hwang [b]

[a] Department of Chemical and Materials Engineering, National Yunlin University of Science and Technology, 123 University Rd., 3 Sec., Douliou, Yunlin 64002, Taiwan, ROC
[b] Graduate Institute of Greenergy Technology, National University of Tainan, Tainan 700, Taiwan, ROC

ARTICLE INFO

Article history:
Received 10 February 2010
Received in revised form 31 March 2010
Accepted 31 March 2010
Available online 9 April 2010

Keywords:
Molten carbonate fuel cell
Start-up operation
Optimization
Preheater
Simulation

ABSTRACT

The study of start-up performance for a direct internal reforming molten carbonate fuel cell (DIR-MCFC) system is presented. Since a kW-class stack is assembled with an additional preheating design, the improvement of start-up behavior is conducted to find the proper operating strategy. For a cold start-up fuel cell system, both start-up delay and inverse response are strictly detected. When the optimum operating strategy is determined by solving the steady-state optimization algorithm subject to stack temperature constraint, the rapid system start-up as well as the maximum power output can be achieved simultaneously.

Crown Copyright © 2010 Published by Elsevier B.V. All rights reserved.

1. Introduction

The molten carbonate fuel cell (MCFC) systems are being considered as one of promising solutions in new energy technologies, because it could provide the higher cell voltage, the better thermal efficiency and the longer life than other fuel cell systems [1]. Hydrogen is ideal fuel for a general class of MCFC systems, but the hydrogen technology in storage, transportation and economic efficiency are not mature yet in the commercial market. At the present stage, alternative fuel sources instead of pure hydrogen through the hydrocarbon steam-reforming process were effective approaches [2]. For high temperature MCFC systems, methane is often treated as the primary fuel. Through internal reforming [3] or pre-reformer [4], the MCFC system could provide the high energy efficiency and low pollutant emissions compared to traditional fossil fuel-based energy systems [5]. Recently, Sundmacher et al. [6] introduced several approaches for an industrial-scale MCFC plant by virtue of modeling, analysis, optimization and control techniques. In general, this industrial-scale system start-up usually took hours and days due to the requirement of too high operating temperature and specified heating demands.

As for determining the proper operating manner and examining quantitative response of the system to different inlet perturbations, the mathematical modeling and simulation for a class of MCFC systems have been investigated [7–9]. Obviously, the steady-state and dynamic characteristics of two-dimensional model through numerical techniques and model reduction method are used to establish a simple simulation model according to various operating conditions. Based on the mathematical modeling, the temperature control of a specified MCFC model for performance improvement was introduced [10], the optimum operating policy was determined by solving a dynamic optimization problem with respect to system efficiencies [11], and the evaluation of energy and exergy efficiencies of an integrated power generation has been addressed in [12].

To study the start-up operation of high temperature fuel cell systems, the dynamic modeling and analysis of different PEM fuel cell systems were widely studied due to the prospective automotive market [13,14]. For most solid oxide fuel cell (SOFC) stack systems, the typical start-up procedure would depend on combustor and heat exchanger for heating of the air and stack. The modeling and thermal dynamics of the SOFC stack during start-up process have been investigated in [15]. Zhou et al. [16] showed that the start-up performance of MCFC stack depended on different temperature and pressure effects. However, the dynamic modeling of the MCFC start-up process according to various operating manner is seldom investigated.

Since the fast start-up design on high temperature fuel cell systems would face some challenges due to different preheating manners and operating conditions, the dynamic modeling of a jacket-integrated DIR-MCFC stack is studied initially. According to a simple heat exchanger structure as a preheater design, the dynamic

* Corresponding author. Tel.: +886 5 5342601; fax: +886 5 5312071.
E-mail address: weiwu@yuntech.edu.tw (W. Wu).

0378-7753/$ – see front matter. Crown Copyright © 2010 Published by Elsevier B.V. All rights reserved.
doi:10.1016/j.jpowsour.2010.03.099

Nomenclature

A_{cell}	effective cell area, cm^2
C_p^s	average stack heat capacity, $J\,g^{-1}\,K^{-1}$
C_p^{hj}	heat capacity of jacket, $J\,g^{-1}\,K^{-1}$
F	Faraday constant (=96485 $C\,mol^{-1}$)
$\bar{h}_i^{in}$	inlet specific enthalpy of species i into the anode, $J\,mol^{-1}$
$\bar{h}_j^{in}$	inlet specific enthalpy of species j into the cathode, $J\,mol^{-1}$
i_{stack}	stack current density, $mA\,cm^{-2}$
n_{cell}	number of cells in the stack
$\dot{N}_a^{in}$, $\dot{N}_c^{in}$	inlet molar flow rate at the anode/cathode, $mol\,s^{-1}$
N_a, N_c	total moles at the anode/cathode, mol
$P_{a,i}$	partial pressure of species i at the anode, Pa
$P_{c,j}$	partial pressure of species j at the cathode, Pa
R	universal gas constant (=8.314 $J\,mol^{-1}\,K^{-1}$)
m_s	total stack mass, g
m_{hj}	mass of steam in the jacket, g
$\dot{m}_{hj}$	mass flow rate of steam in the jacket, $g\,s^{-1}$
R_t	thermal resistance of the stack, $K\,W^{-1}$
T_{amb}	ambient temperature, K
UA	product of the overall heat transfer coefficient and heat transfer area, $W\,K^{-1}$
$x_{a,i}^{in}$	inlet mole fraction of species i into the anode
$x_{c,j}^{in}$	inlet mole fraction of species j into the cathode

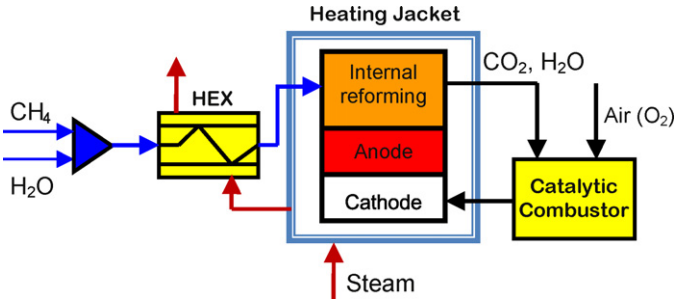

Fig. 1. The run schematic of the DIR-MCFC stack start-up operation.

simulation for the DIR-MCFC stack would be conducted to study the system start-up operation. For a cold start-up system, both start-up delay and inverse response would strongly increase difficulties on the development of control system. To address the rapid system start-up as well as the maximum power output, the optimal operating condition depends on undetermined jacket temperature and steam-to-carbon ratio. Through the steady-state optimization algorithm subject to the upper limit of stack operating temperature, the optimum air flow rate is obtained which is verified by simulation results.

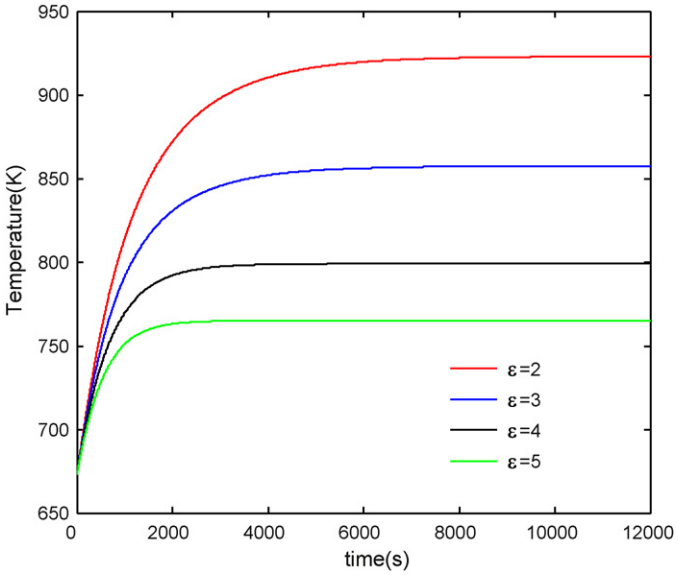

Fig. 2. No preheating: the stack temperature responses under different steam-to-carbon ratios.

2. System description

Inspired by a 250 kW class of MCFC stack where the anode and cathode gas recirculation manners were utilized to recover waste heat as well as improve the power efficiency [17], the new heat integration design for the MCFC stack system is depicted in Fig. 1. At the room temperature (298 K), the cold mixture of methane and water is preheated by a traditional heat exchanger (HEX) and then the heated mixture with specified steam-to-carbon ratio is directly fed into the internal reforming unit. In the meanwhile, the stack temperature is perheated by a jacket with inlet hot steam until the start-up temperature for the reforming process is achieved at 673 K at least. Afterwards, the feed would be converted into hydrogen rich gas mixture via the following two reactions:

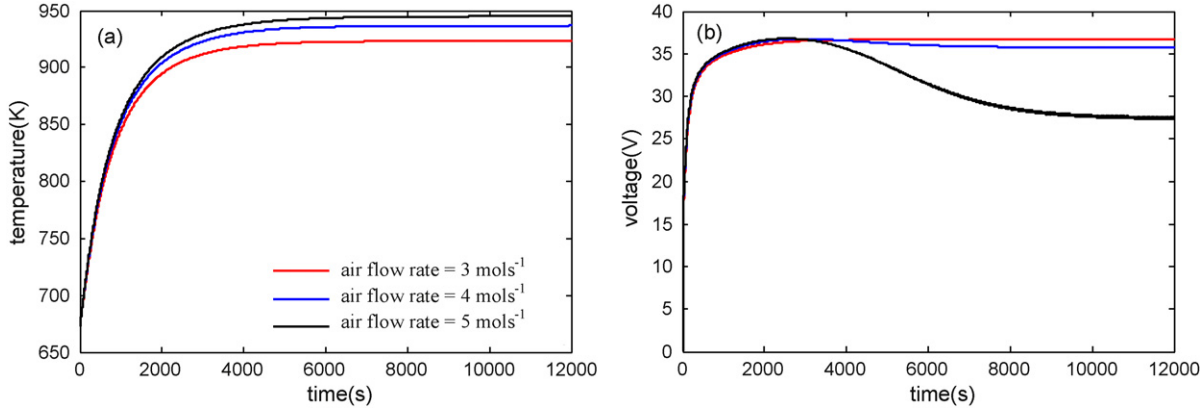

Fig. 3. For a hot start-up system under different air flow rates: (a) stack temperature responses and (b) corresponding stack voltage.

Table 1
Kinetic parameters of reforming reactions.

$A_R = 3.71 \times 10^{17}$	$\Delta E_R = 240.1\ \mathrm{kJ\ mol^{-1}}$
$A_W = 5.43$	$\Delta E_W = 67.13\ \mathrm{kJ\ mol^{-1}}$
$B_{CH_4} = 6.65 \times 10^{-9}$	$\Delta H_{CH_4} = -38.28\ \mathrm{kJ\ mol^{-1}}$
$B_{H_2O} = 1.77 \times 10^{5}$	$\Delta H_{H_2O} = 88.68\ \mathrm{kJ\ mol^{-1}}$
$B_{H_2} = 6.12 \times 10^{-14}$	$\Delta H_{CO} -70.65\ \mathrm{kJ\ mol^{-1}}$
$B_{CO} = 8.23 \times 10^{-10}$	$\Delta H_{H_2} = -82.9\ \mathrm{kJ\ mol^{-1}}$

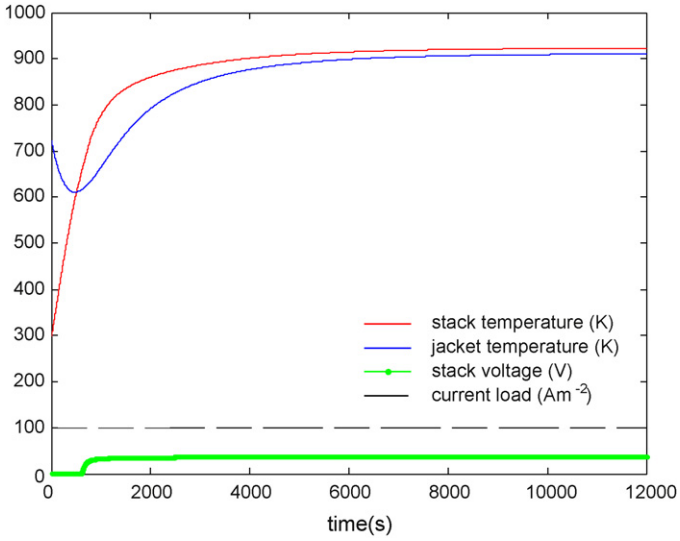

Fig. 4. For a cold start-up system: the responses of stack, jacket temperatures and stack voltage.

(i) Steam/methane reforming reaction:

$$CH_4 + H_2O \overset{r_R}{\longleftrightarrow} CO + 3H_2, \quad \Delta H^{\circ}_{298} = 206\ \mathrm{kJ\ mol^{-1}} \tag{1}$$

(ii) Water–gas shift reaction:

$$CO + H_2O \overset{r_W}{\longleftrightarrow} CO_2 + H_2, \quad \Delta H^{\circ}_{298} = -41\ \mathrm{kJ\ mol^{-1}} \tag{2}$$

where both rate equations r_R and r_w are shown in Eqs. (A1) and (A2). Under an external current demand, the half-cell reactions take place in anode and cathode electrodes, respectively (Table 1),

Anode:

$$H_2 + {CO_3}^{2-} \rightarrow CO_2 + H_2O + 2e^- \tag{3}$$

Cathode:

$$\frac{1}{2}O_2 + CO_2 + 2e^- \rightarrow {CO_3}^{2-} \tag{4}$$

The overall cell reaction occurs in a homogenous layer to produce electricity and heat simultaneously. The anode exhaust gas is fully oxidized with the excess air in a catalytic combustor and then the produced carbon dioxide with oxygen is fed into the cathode channel. The outlet jacket steam flows into the external HEX to warm-up the fresh mixture of methane and water. In our proposed

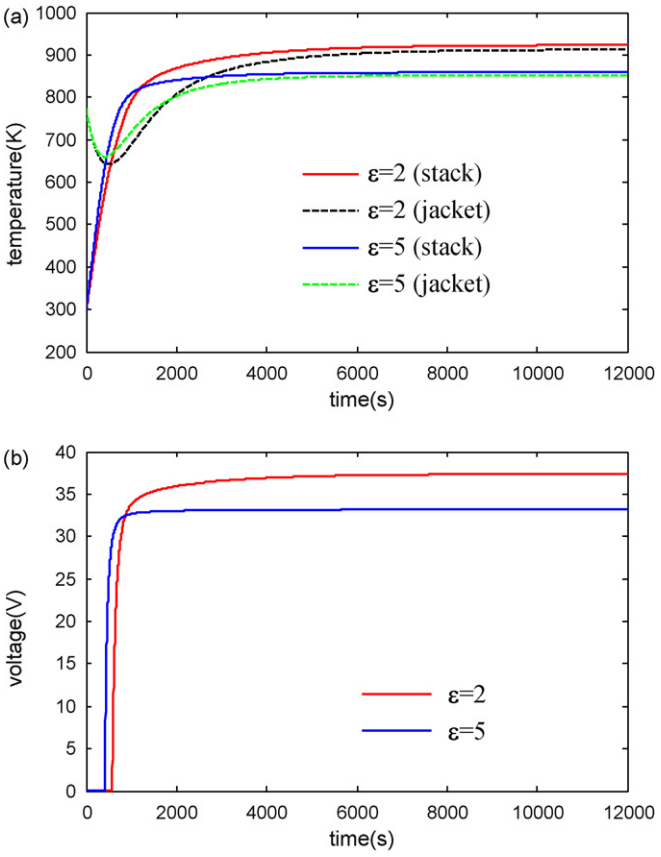

Fig. 5. For a cold start-up system under different steam-to-carbon ratio: (a) stack temperature responses and (b) corresponding stack voltage.

system configuration, some general assumptions and start-up conditions are noticed as follows:

(i) Gas mixtures at inlet/outlet flows of the stack are ideal mixtures.
(ii) Thermodynamic properties follow the ideal gas law.
(iii) Energy accumulates only in the stack solid mass.
(iv) The outlet flow temperatures of the DIR-MCFC stack are equal to the stack temperature, and the outlet jacket temperature is equal to the jacket temperature.
(v) There is no phase transition between water and steam in the inside of DIR-MCFC stack.
(vi) There are no concentration, velocities and temperature gradients perpendicular to the direction of gas flow.
(vii) The anode and cathode are well mixed volumes with interchange of carbonate ions through the electrolyte matrix separating the two sides.
(viii) The hot steam is fed into the heating jacket and the exhaust steam flows into the HEX.
(ix) During the stack start-up period, the heating jacket instead of HEX acts to heat the mixture of methane and water at the

Table 2
Heat capacity coefficients for species from 298 to 1500 K at constant pressure.

Species	$\bar{h}^{ref}$ (kcal mol^{-1})	a (cal K^{-1} mol^{-1})	b ($\times 10^{-3}$ cal K^{-1} mol^{-1})	c ($\times 10^{-8}$ cal K^{-1} mol^{-1})
H_2	0.000	6.947	−0.200	0.481
O_2	0.000	6.148	3.102	−0.923
H_2O	−57.800	7.256	2.298	0.283
CO_2	−94.054	6.214	10.396	−3.545
CO	−26.417	6.420	1.665	−0.196
CH_4	−17.895	3.381	18.044	−4.300

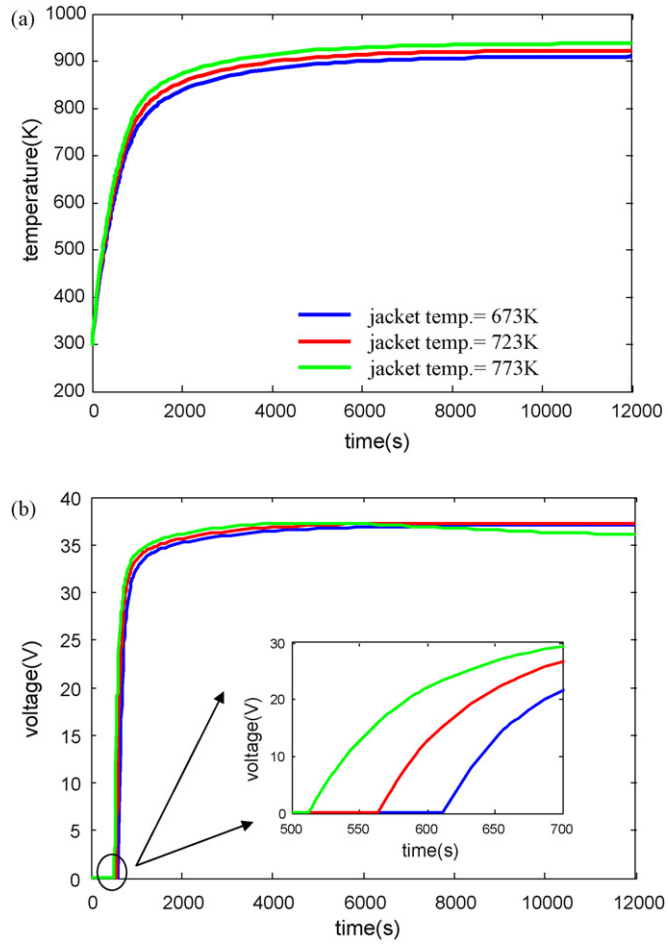

Fig. 6. For a cold start-up system under different jacket temperatures: (a) stack temperature responses and (b) corresponding stack voltage.

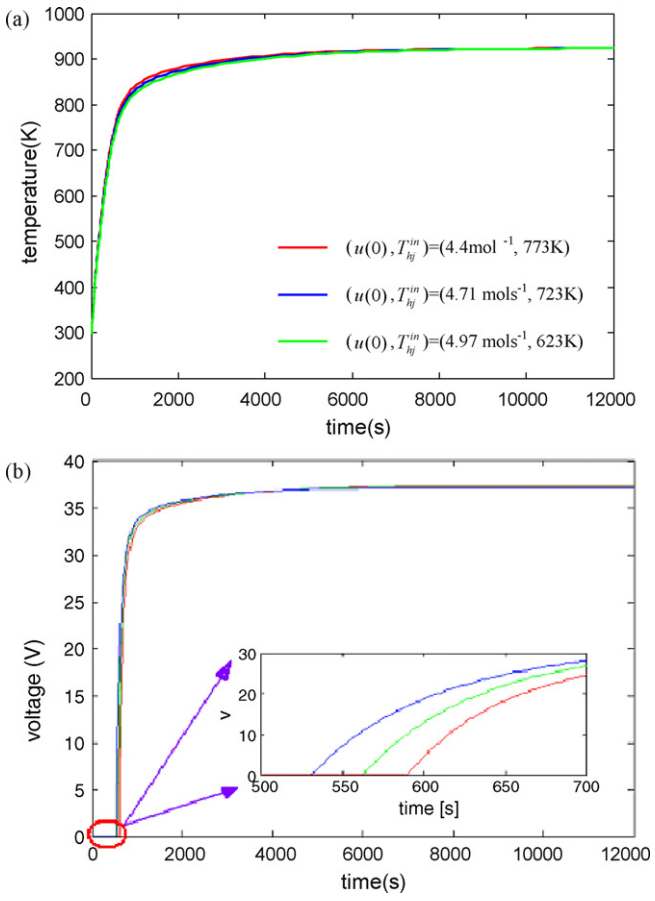

Fig. 7. For a cold start-up system with specified $\varepsilon = 2$: (a) stack temperature responses under different jacket temperatures and prescribed air flow rate and (b) corresponding stack voltage.

anode, and meanwhile the air is heated with the heating jacket at the cathode.

(x) For the sake of simplicity, the dynamics of external devices including HEX and catalytic combustor are omitted.

(xi) The overall system is a continuous process from start-up stage to steady-state operation.

According to above statements, the dynamic modeling of DIR-MCFC is introduced in Appendix A. The state–space representation of the DIR-MCFC system is described by:

$$\begin{aligned} \dot{\xi} &= F(\xi, \delta) \\ y &= h(\xi) \end{aligned} \tag{5}$$

where the state $\xi = [x_{a,i}, x_{c,j}, T_{hj}^{\text{out}}, T]^T$ represents species i (Table 2) at the anode, species j at the cathode, jacket temperature and stack temperature. The non-linear vector function F is constructed from Eqs. (A1)–(A13). $\delta = [x_{a,\text{CH}_4}^{\text{in}}, x_{a,\text{H}_2\text{O}}^{\text{in}}, x_{c,\text{O}_2}^{\text{in}}, T_{hj}^{\text{in}}]^T$ represents the inlet mixture of methane and water at the anode, air (oxygen) flow rate at the cathode and inlet jacket temperature, respectively. The cell voltage is denoted as the output variable $y = V_{\text{cell}}$, and the corresponding output function $h(\xi)$ is formulated by Eqs. (A14)–(A16).

Remark 1. Basically, the state–space model in Eq. (5) is used to describe the dynamic behavior of jacket-integrated DIR-MCFC stack regardless of the system start-up. If the preheating procedure is neglected, and the temperature and pressure of the experiment-based DMFC reliably range from 673 to 923 K and 1–3 atm, respectively, then the system responses with respect to the current demand are investigated by the following simulation results

- If the inlet flows of the system is heated up to the lower limit of stack operating temperature, i.e. $T_{\text{min}} = 673$ K, Fig. 2 depict the stack temperature responses with respect of different steam-to-carbon ratios, $\varepsilon \equiv x_{a,\text{H}_2\text{O}}^{\text{in}}/x_{a,\text{CH}_4}^{\text{in}}$ at a constant air (O_2) flow rate $\dot{N}_c^{\text{in}} x_{c,\text{O}_2}^{\text{in}} = 4\,\text{mol}\,\text{s}^{-1}$. Since the steam-reforming of methane is an endothermic process, the conversion of methane is limited by chemical equilibrium and temperature effect. Therefore, the large steam-to-carbon ratio induces the lower stack temperature at steady-state due to a large amount of water.
- In this case of dynamic model of the MCFC stack, the desired operating temperature is 923 K. At a temperature lower than 773 K, the cell performance drops significantly, while a temperature higher than 923K accelerates material corrosion and power loss. Under a given steam-to-carbon ratio $\varepsilon = 2$, Fig. 3(a) shows that the increase of air flow rate can increase stack temperature. According to the upper limit of the stack temperature, i.e. $T_{\text{max}} = 923$ K, Fig. 3(b) demonstrates significantly voltage drop in the cell circuit while the air flow rate is more than $4\,\text{mol}\,\text{s}^{-1}$.

Apparently, the operating temperature strictly affects the stack performance, and the improper steam-to-carbon ratio or air flow rate induces significant voltage drop.

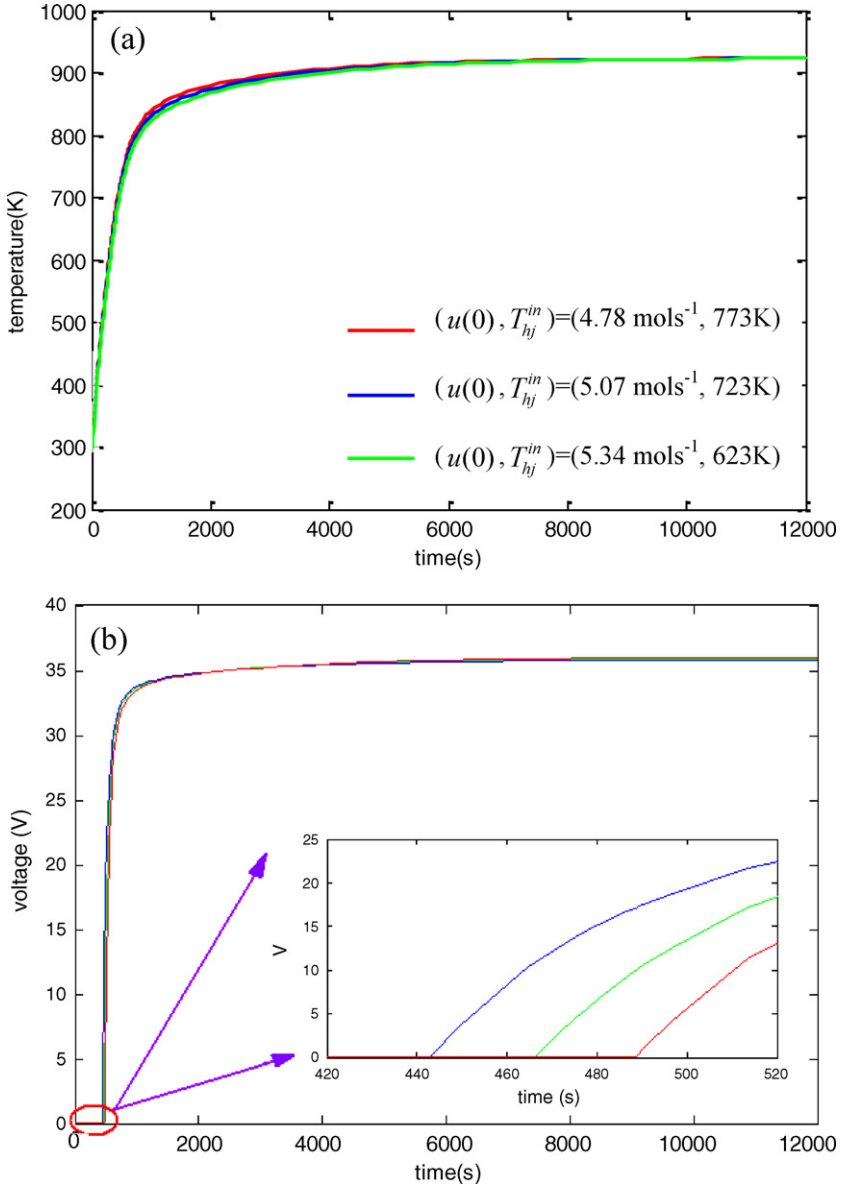

Fig. 8. For a cold start-up system with specified $\varepsilon = 3$: (a) stack temperature responses under different jacket temperatures and prescribed air flow rate and (b) corresponding stack voltage.

3. System start-up performance

Actually, the preheating procedure is essential when the stack temperature is lower than the normal operating temperature. To address the start-up model of the jacket-integrated DIR-MCFC model, the state–space equation in Eq. (5) is reduced to

$$\dot{\eta} = q(\eta, \delta),\ 0 \le t < t_r \tag{6}$$

where the warm-up period $t_r > 0$, the state $\eta = [T_{hj}^{\text{out}}, T]^T$ and the vector function q by Eqs. (A10) and (A12) is rewritten as:

$$q = \begin{bmatrix} \dfrac{\dot{m}_{hj}}{m_{hj}}\left(T_{hj}^{\text{in}} - T_{hj}^{\text{out}}\right) - \dfrac{Q_{\text{heat}}}{m_{hj}C_p^{hj}} \\ \dfrac{\dot{N}_a^{\text{in}}\sum_{i\in S_a} x_{a,i}^{\text{in}}\left(\bar{h}_i^{\text{in}} - \bar{h}_i\right) + \dot{N}_c^{\text{in}}\sum_{i\in S_c} x_{c,j}^{\text{in}}\left(\bar{h}_j^{\text{in}} - \bar{h}_j\right) - (T - T_{\text{amb}})/R_t + Q_{\text{heat}}}{m_s C_p^s + (E_{a,h} + E_{c,h})/T} \end{bmatrix} \tag{7}$$

and its initials $\eta(0) = \left[T_{hj}^{\text{in}}, T_{\text{ref}}\right]$.

Remark 2. According to above start-up model, there are no electrochemical reactions in the cell during a warm-up period. The heating jacket carries out the preheating procedure including heating mixture of methane and water and air flow rate at the anode/cathode as well. However, the warm-up period is uncertain due to variety of inlet conditions. In Eq. (7), the steam-to-carbon ratio, air flow rate and inlet jacket temperature dominate the transient behavior of the start-up model. Furthermore, the preheating and start-up operation via the dynamic simulation are discussed as follows:

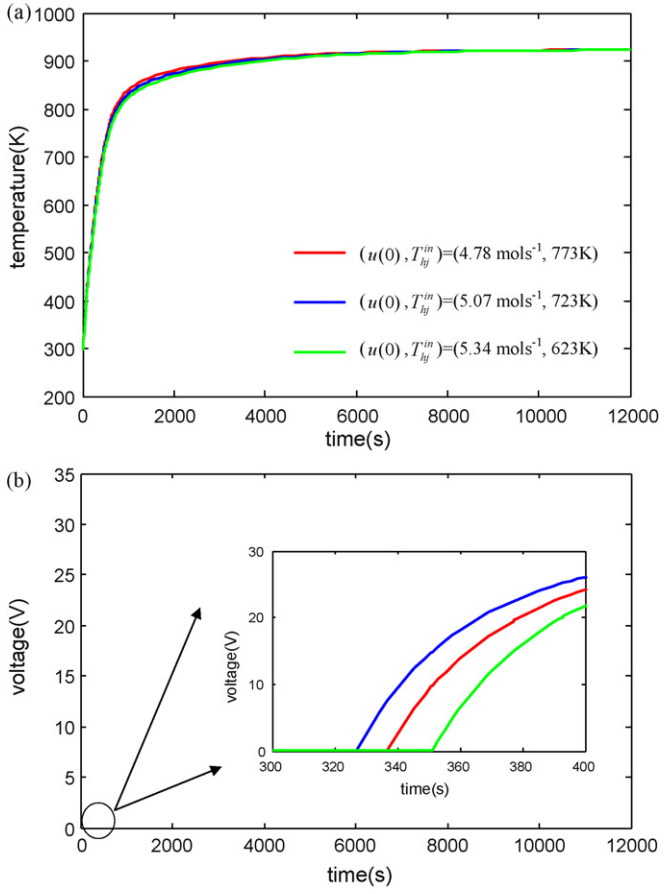

Fig. 9. For a cold start-up system with specified $\varepsilon = 5$: (a) stack temperature responses under different jacket temperatures and prescribed air flow rate and (b) corresponding stack voltage.

- When initial temperatures of inlet flows are 298 K, Fig. 4 shows profiles of the stack temperature, jacket temperature and stack voltage, respectively, under the inlet conditions including $T_{hj}^{\text{in}} = 723\,\text{K}$, $\varepsilon = 2$, $\dot{N}_c^{\text{in}} x_{c,\text{O}_2}^{\text{in}} = 4\,\text{mol}\,\text{s}^{-1}$ and $i_{\text{stack}} = 100\,\text{A}\,\text{m}^{-2}$. During the start-up period, the warm-up period is estimated while the stack temperature approaches to $T_{\min}$ (673 K) and the system start-up delay is equivalent to t_r. Since the jacket is a simple heat transfer device, it is treated as the preheater in the start-up period but it may become a cooling device while the stack temperature is higher than the jacket temperature. Therefore, the inverse response appears due to a change of sign of temperature difference between jacket and stack at the start-up and steady-state stages, respectively.
- Under $T_{hj}^{\text{in}} = 723\,\text{K}$ and $\dot{N}_c^{\text{in}} x_{c,\text{O}_2}^{\text{in}} = 3\,\text{mol}\,\text{s}^{-1}$, Fig. 5(a) shows the responses of stack and jacket temperatures under various steam-to-carbon ratios. The corresponding stack voltage responses are depicted in Fig. 5(b). Notably, the small value of ε can increase system temperature and enhance the stack voltage at steady-state operation, but the corresponding start-up delay is obvious. Apparently, different carbon-to-steam ratios may encounter the trade-off between small start-up delay and large power output.
- Under $\varepsilon = 2$ and $\dot{N}_c^{\text{in}} x_{c,\text{O}_2}^{\text{in}} = 3\,\text{mol}\,\text{s}^{-1}$, Fig. 6(a) shows the stack temperature responses under various inlet jacket temperatures. Notably, the increase of inlet jacket temperature can gradually increase the stack temperature and meanwhile reduce the start-up delay depicted by the zoom-out plot in Fig. 6(b). However, the highest jacket temperature, e.g. $T_{hj}^{\text{in}} = 723\,\text{K}$, would induce voltage drop at steady-state due to the steady-state stack temperature more than $T_{\max}$ (923 K).

Table 3
Optimum air flow rates.

Inlet condition	Air flow rate $u(0)$ (mol s^{-1})
$\varepsilon = 2$, $T_{hj}^{\text{in}} = 673\,\text{K}$	4.97
$\varepsilon = 2$, $T_{hj}^{\text{in}} = 723\,\text{K}$	4.71
$\varepsilon = 2$, $T_{hj}^{\text{in}} = 723\,\text{K}$	4.4
$\varepsilon = 3$, $T_{hj}^{\text{in}} = 673\,\text{K}$	5.34
$\varepsilon = 3$, $T_{hj}^{\text{in}} = 723\,\text{K}$	5.07
$\varepsilon = 3$, $T_{hj}^{\text{in}} = 723\,\text{K}$	4.78
$\varepsilon = 5$, $T_{hj}^{\text{in}} = 673\,\text{K}$	6.67
$\varepsilon = 5$, $T_{hj}^{\text{in}} = 723\,\text{K}$	6.41
$\varepsilon = 5$, $T_{hj}^{\text{in}} = 723\,\text{K}$	6.12

By above simulation study, the stack start-up delay and the stack voltage are all affected by varieties of carbon-to-steam ratio and inlet jacket temperature. However, a rapid system start-up operation may induce a low power output or voltage drop.

4. Optimum operating conditions

Referring previous simulation tests, the high stack temperature can improve the power performance, but the too high stack temperature, i.e. $T > T_{\max}$, would induce significant voltage drop. We found that the variety of inlet conditions including carbon-to-steam ratio (ε), inlet jacket temperature (T_{hj}^{in}) and air flow rate ($\dot{N}_c^{\text{in}} x_{c,\text{O}_2}^{\text{in}}$) strongly affect the stack temperature in a steady-state operation as well as stack start-up delay in a start-up operation. To address a rapid system start-up operation, i.e. small start-up delay, and also achieve the desired stack temperature in a steady-state operation, the optimum operating strategy is an essential approach. Moreover, a combination of jacket-integrated DIR-MCFC and start-up model is described by:

$$\begin{cases} \dot{\eta} = q(\eta, \delta), & 0 \le t < t_r \\ \dot{\xi} = F(\xi, \delta), & t \ge t_r \end{cases} \tag{8}$$

where $\eta(0) = \left[T_{hj}^{\text{in}}, T_{\text{ref}}\right]$ and $\xi(t_r) = [x_{a,i}^{\text{in}}, x_{c,j}^{\text{in}}, T_{hj}^{\text{out}}, T_{\min}]^T$. Obviously, the inlet conditions of δ would dominate the overall dynamic behavior and the start-up delay. Since a rapid start-up operation may cause the degradation of stack performance due to improper carbon-to-steam ratio and too high stack temperature, the optimum start-up operating policy is required under a steady-state optimization framework. Moreover, the minimization of the following objective function subject to system constraints is shown by:

$$\min_{u(0)} J = (T_{ss} - T_{\max})^2 \tag{9}$$

s.t.,

$$\begin{aligned} 0 &= F(\xi_{ss}, u(0)) \\ T_{\min} &\le T_{ss} \le T_{\max} \end{aligned} \tag{10}$$

where the initial condition $u(0) \in \left\{\varepsilon, N_c^{\text{in}} x_{c,\text{O}_2}^{\text{in}}, T_{hj}^{\text{in}}\right\}$ and ξ_{ss} represents the stack steady-state value. Notably, it is typically non-linear programming (NLP) problem to find the solution $u(0)$. The solver from Matlab Optimization Toolbox® is used.

Remark 3. According to the optimization algorithm, one of inlet conditions can be obtained via the numerical computation in the Matlab environment. The off-line iteration is used to find the minimization of single objective in a steady-state operation, i.e. $\lim_{t\to\infty} T = T_{\max}$. In Table 3, optimum air flow rates $u(0)$, are obtained according to various inlet jacket temperatures $T_{hj}^{\text{in}} = 673,\ 723,\ 773\,\text{K}$, and a given steam-to-carbon ratio $\varepsilon \in \{2,\ 3,\ 5\}$. The dynamic responses of stack temperature and stack voltage are depicted in Figs. 7–9,

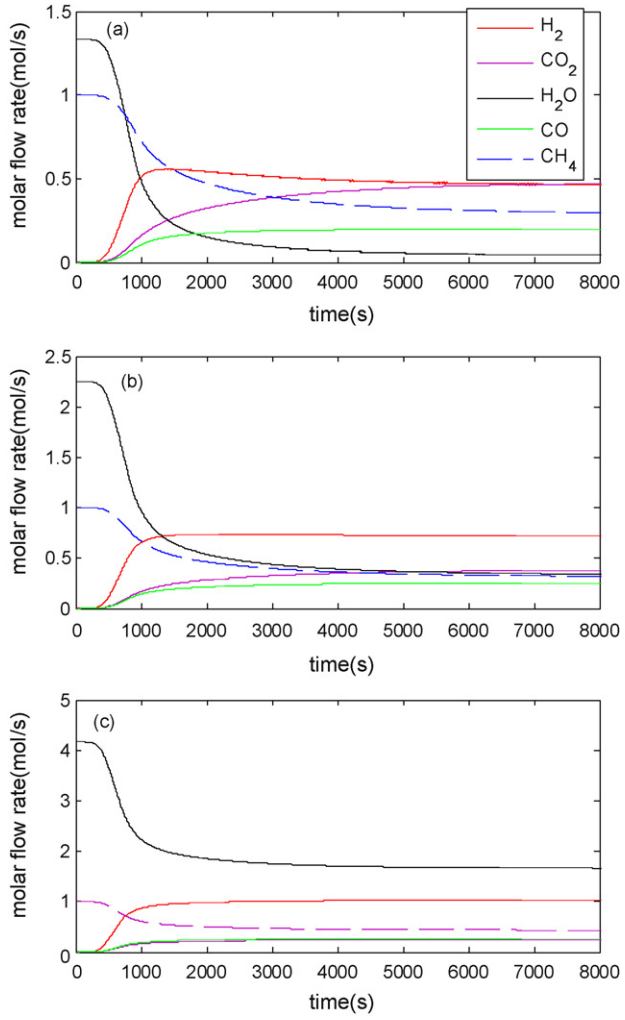

Fig. 10. The responses of molar flow rates of each component in the stack at different operating conditions: (a) $(\varepsilon, N_c^{in}x_{c,O_2}^{in}, T_{hj}^{in}) = (2, 4.97, 673)$; (b) $(\varepsilon, N_c^{in}x_{c,O_2}^{in}, T_{hj}^{in}) = (3, 5.34, 673)$; (c) $(\varepsilon, N_c^{in}x_{c,O_2}^{in}, T_{hj}^{in}) = (5, 6.67, 673)$.

respectively. Moreover, the analysis and discussion of optimum start-up strategy is stated as follows:

- All stack temperatures are close to the upper limit of operating temperature as time approaches sufficiently large, and meanwhile all stack voltages are kept at the highest level without any voltage drop.
- The stack start-up response can be accessed from the zoom-out of each stack voltage response. At inlet jacket temperatures $T_{hj}^{in} = 723$ K, the high steam-to-carbon ratio can reduce start-up delay.
- The amount of water flow strongly affects the impedance for anode overpotential, so the higher steam-to-carbon ratio would induce the lower voltage output.

Consequently, the system start-up as well as the power performance can be improved simultaneously by the evaluation of inlet conditions $(\varepsilon,\ N_c^{in}x_{c,O_2}^{in}, T_{hj}^{in})$. Besides, the responses of some species in the DIR-MCFC with prescribed operating condition are shown in Fig. 10(a)–(c). Notably, Fig. 10(c) shows that the high steam-to-carbon ratio induces a larger amount of hydrogen but a lower amount of CO. It stated that the operating condition for the stack system would not be prone to carbon monoxide "poisoning". In the presented preheating configuration, it provides a prospective alternative to improve the stack start-up operation. In fact, too short warm-up period for a scale-up power system is probably unrealistic and absolute challenge.

5. Conclusions

In this article, the new heat integration configuration of the DIR-MCFC system is proposed. The heating jacket is denoted as an additional heat exchanger. Regarding the start-up operation, the start-up delay and inverse response are investigated via the dynamic simulation. The manipulation of steam-to-carbon ratio, air flow rate and inlet jacket temperature could dominate the stack start-up operation. The steady-state optimization algorithm is successfully employed. Under optimum air flow rate with respect to prescribed inlet conditions, the system start-up delay is improved while the maximum power output is achieved. Basically, the optimum initial condition is not unique and depends on specified operating constraints. With aid of dynamic simulation and evaluation procedure, the system start-up delay is not only reduced but the satisfactory power performance is also guaranteed.

Acknowledgments

The authors would like to thank the National Science Council of the Republic of China for financially supporting this research under Contract No. NSC 98-2622-E-224-025-CC3.

Appendix A.

Assume that both reversible reactions in Eqs. (1) and (2) obey the laws of chemical equilibrium, the rate equations r_R and r_w are formulated by [4,18]:

$$r_R = \frac{A_R \exp(-\Delta E_R/RT)[(P_{CH_4}P_{H_2O}/P_{H_2}^{2.5}) - (P_{H_2}^{0.5}P_{CO}/K_{Re})]}{DEN^2} \quad (A1)$$

$$r_w = \frac{A_w \exp(-\Delta E_w/RT)[(P_{CO}P_{H_2O}/P_{H_2}) - (P_{CO_2}/K_{We})]}{DEN^2} \quad (A2)$$

where,

$$DEN = 1 + B_{CO}\exp(-\Delta H_{CO}/RT)P_{CO} + B_{H_2}\exp(-\Delta H_{H_2}/RT)P_{H_2} + B_{CH_4}\exp(-\Delta H_{CH_4}/RT)P_{CH_4} + B_{H_2O}\exp(-\Delta H_{H_2O}/RT)P_{H_2O}P_{H_2}^{-1} \quad (A3)$$

and equilibrium constants are given by:

$$K_{Re} = 1.03 \times 10^{10} \exp\left[30.4197 - \frac{27106.2}{T}\right] \quad (A4)$$

$$K_{We} = \exp\left[-3.79762 + \frac{4159.54}{T}\right] \quad (A5)$$

Notably, above values of rate factors for the internal reforming unit is listed in Table 1. The rate for the electrochemical reactions at the anode and cathode in Eqs. (3) and (4) are given by the Faraday's law of electrolysis:

$$r_e = \frac{i_{stack}A_{cell}n_{cell}}{2F} \quad (A6)$$

Inspired by the dynamic modeling of DIR-MCFC in some literatures [11,19], the mole balance equations for the electrochemical half reaction at the anode are described by:

$$\dot{x}_{a,i} = (N_a)^{-1}\left[\dot{N}_a^{in}\left(x_{a,i}^{in} - x_{a,i}\right) - x_{a,i}(2r_R + r_e) + R_{a,i}\right] \quad (A7)$$

where the species $i \in S_a \equiv \{H_2, CH_4, CO, CO_2, H_2O\}$ and $R_a = [3r_R + r_W - r_e, -r_R, r_R - r_W, r_W + r_e, -r_R - r_W]$. The electrochemical half reaction at the cathode is modeled by:

$$\dot{x}_{c,j} = (N_c)^{-1}\left[\dot{N}_c^{in}\left(x_{c,j}^{in} - x_{c,j}\right) + 1.5x_{c,j}r_e + R_{c,j}\right] \quad (A8)$$

where the species $j \in S_c \equiv \{CO_2, O_2\}$, and $R_c = [-r_e, -0.5r_e]$. Since the stack is completely covered by heating jacket, the heat transfer rate between the stack and heating jacket is simplified by [20]:

$$Q_{heat} = UA\frac{(T_{hj}^{in} - T) - (T_{hj}^{out} - T)}{\ln\left(\frac{T_{hj}^{in} - T}{T_{hj}^{out} - T}\right)} \quad (A9)$$

and the heating jacket is modeled by:

$$\frac{dT_{hj}^{out}}{dt} = \frac{\dot{m}_{hj}}{m_{hj}}\left(T_{hj}^{in} - T_{hj}^{out}\right) - \frac{Q_{heat}}{m_{hj}C_p^{hj}} \quad (A10)$$

where T_{hj}^{in} and T_{hj}^{out} represent the inlet and outlet steam temperature, respectively. The heat capacity of steam is formulated by:

$$C_p^{hj} = 7.256 + 2.298 \times 10^{-3}T_{hj}^{out} + 2.83 \times 10^{-9}\left(T_{hj}^{out}\right)^2 \quad (A11)$$

Under assumptions (i)–(vii), the thermal model of the stack is described by a first-order differential equation:

$$\frac{dT}{dt} = \frac{E_{a,g} + E_{c,g} - (T - T_{amb})/R_t - V_{cell}i_{stack} + Q_{heat}}{m_sC_p^s + (E_{a,h} + E_{c,h})/T} \quad (A12)$$

where $E_{a,h} = \dot{N}_a^{in}\sum_{i\in S_a}x_{a,i}\bar{h}_i$, $E_{c,h} = \dot{N}_c^{in}\sum_{j\in S_c}x_{c,j}\bar{h}_j$, $E_{a,g} = \dot{N}_a^{in}\sum_{i\in S_a}(x_{a,i}^{in}\bar{h}_i^{in} - x_{a,i}\bar{h}_i) - \sum_{i\in S_a}x_{a,i}\bar{h}_i\sum_{i\in S_a}R_{a,i}$ and $E_{c,g} = \dot{N}_c^{in}\sum_{j\in S_c}\left(x_{c,j}^{in}\bar{h}_j^{in} - x_{c,j}\bar{h}_j\right) - \sum_{j\in S_c}x_{c,j}\bar{h}_j\sum_{i\in S_c}R_{c,j}$. The specific enthalpies of species at the anode and cathode, are written by:

$$\bar{h}_k = \bar{h}_k^{ref} + \int_{T_{ref}}^{T}\left(a_k + b_ku + c_ku^2\right)du,\ k \in \{S_a, S_c\} \quad (A13)$$

where the value of each $\bar{h}_k^{ref}$ and coefficients for each component are listed in Table 2. Finally, the performance of fuel cell is evaluated by the cell voltage under a specified current demand. The cell voltage of DIR-MCFC consists of equilibrium cell potential, cell overpotentials and cell resistance:

$$V_{cell} = E_{eq} - i_{stack}(\eta_{ohm} + \eta_a + \eta_c) \quad (A14)$$

where the equilibrium cell potential is described by:

$$E_{eq} = \frac{2.44 \times 10^5 - (472.45 + 0.04T)T}{2F} + \frac{RT}{2F}\ln\frac{P_{a,H_2}P_{c,CO_2}P_{c,O_2}^{0.5}}{P_{a,CO_2}P_{a,H_2O}} \quad (A15)$$

Cell overpotentials are based on the following empirical equations [21] to describe anode and cathode overpotentials:

$$\eta_a = 2.27 \times 10^{-9}\exp\left(\frac{6435}{T}\right)P_{a,H_2}^{-0.42}P_{a,CO_2}^{-0.17}P_{a,H_2O}^{-1}$$
$$\eta_c = 7.505 \times 10^{-10}\exp\left(\frac{9298}{T}\right)P_{c,O_2}^{-0.43}P_{c,CO_2}^{-0.09} \quad (A16)$$

Cell resistance which contributes to the ohmic loss is expressed with the Arrhenius equation [22]:

$$\eta_{ohm} = 0.5 \times 10^{-4}\exp\left[3016\left(\frac{1}{T} - \frac{1}{923}\right)\right] \quad (A17)$$

References

[1] P. Tomczyk, J. Power Sources 160 (2006) 858–862.
[2] N. Sammes, Fuel Cell Technology: Reaching Towards Commercialization, Springer-Verlag, London, 2006.
[3] P. Heidebrecht, K. Sundmacher, Fuel Cells 2 (2002) 166–180.
[4] M. Mangold, M. Sheng, Fuel Cells 4 (2004) 68–77.
[5] N.V. Khartchenko, Advanced Energy Systems, Taylor & Francis, USA, 1998.
[6] K. Sundmacher, A. Kienle, H.J. Pesch, J.F. Berndt, G. Huppmann, Molten Carbonate Fuel Cells: Modeling, Analysis, Simulation, and Control, Wiley, London, 2007.
[7] M.D. Lukas, K.Y. Lee, Fuel Cells 5 (2005) 115–125.
[8] M. Fermeglia, A. Gudicio, G. DeSimon, G. Longo, S. Pricl, Fuel Cells 5 (2005) 66–79.
[9] H. Hao, H. Zhang, S. Weng, M. Su, J. Power Sources 161 (2006) 849–855.
[10] F. Yang, X.J. Zhu, G.-Y. Cao, J. Power Sources 164 (2007) 713–720.
[11] S. Kameswaran, L.T. Biegler, S.T. Junker, H. Ghezel-Ayagh, AIChE J. 53 (2007) 460–474.
[12] R. Rashidia, P. Bergb, I. Dincer, Int. J. Hydrogen Energy 34 (2009) 4395–4405.
[13] H. Meng, J. Power Sources 178 (2008) 141–150.
[14] S.J. Andreasen, S.K. Kær, Int. J. Hydrogen Energy 33 (2008) 4655–4664.
[15] J. Ki, D. Kim, J. Power Sources 195 (2010) 3186–3200.
[16] L. Zhou, H. Lin, B. Yi, H. Zhang, Z. Shao, P. Ming, M. Cheng, Electrochim. Acta 51 (2006) 5689–5702.
[17] A.F. Au, S.J. McPhail, N. Woudstra, K. Hemmes, J. Power Sources 122 (2003) 37–46.
[18] J. Li, Y.-W. Kang, G.-Y. Cao, X.-J. Zhu, H.-Y. Tu, J. Li, J. Power Sources 179 (2008) 673–682.
[19] F. Yang, X.-J. Zhu, G.-Y. Cao, J. Power Sources 166 (2007) 354–361.
[20] M.T. Dhotre, Z.V.P. Murthy, N.S. Jayakumar, Chem. Eng. J. 118 (2006) 183–188.
[21] C.Y. Yuh, J.R. Selman, J. Electrochem. Soc. 138 (1991) 3642–3648.
[22] J.-H. Koh, B.S. Kang, H.C. Lim, AIChE J. 47 (2001) 1941–1956.